geosciences

MDPI

Article

Physicochemical and Geotechnical Alterations to MX-80 Bentonite at the Waste Canister Interface in an Engineered Barrier System

Christopher W. Davies [1,*], Colin T. Davie [2], Edward A. Charles [3] and Maggie L. White [3]

1 AECOM, Environment and Ground Engineering, Newcastle upon Tyne NE1 2HF, UK
2 School of Civil Engineering and Geosciences, Newcastle University, Newcastle upon Tyne NE1 7RU, UK; colin.davie@newcastle.ac.uk
3 School of Chemical Engineering and Advanced Materials, Newcastle University, Newcastle upon Tyne NE1 7RU, UK; alasdair.charles@newcastle.ac.uk (E.A.C.); maggie.white@newcastle.ac.uk (M.L.W.)
* Correspondence: Christopher.Davies@aecom.com

Received: 2 May 2017; Accepted: 18 July 2017; Published: 10 August 2017

Abstract: The study investigated the basic geomechanical and mineralogical evolution of the bentonite barrier under various experimental boundary conditions which replicated the near-field Thermo-Hydro-Chemico (THC) conditions in a repository. The relationships between the physicochemical alterations and changes in the geotechnical properties have seldom been studied, especially on a consistent dataset. This paper attempts to link the physicochemical properties of Na-bentonite (MX-80) to the macro-scale engineering functionality of the bentonite post THC exposure. Experiments investigated the impact of THC variables on the engineering and physicochemical functionality of the bentonite with respect to its application within a High-Level Waste (HLW) engineered barrier system. Intrinsic alterations to the MX-80 bentonite under relatively short-term exposure to hydrothermal and chemical conditions were measured. Additionally, two long-term tests were conducted under ambient conditions to consider the impact of exposure duration. The intrinsic measurements were then related to the overall performance of the bentonite as a candidate barrier material for application in a UK geological disposal facility. Findings indicate that exposure to thermo-saline-corrosion conditions (i.e., corrosion products derived from structural grade 275 carbon steel) inhibits the free swell capacity and plasticity of the bentonite. However, the measured values remained above the design limits set out for the Swedish multi-barrier concept, from which the UK concept may take a lead. Corrosion alone does not appear to significantly affect the geotechnical measurements compared with the influence of thermal loading and high saline pore water after relatively short-term exposure. Thermal and corrosion exposure displayed no impact on the intrinsic swelling of the smectite component, indicating that no significant structural alteration had occurred. However, when exploring more complex saline solutions i.e., mixed Na, K and Ca, rather than the reference NaCl, divalent cation replacement was observed within the interlayer exchange site. This was accelerated in higher thermal loading conditions.

Keywords: Thermo-Hydro-Chemico; MX-80; near-field; corrosion; saline; multi-barrier; geological disposal facility; high level waste

1. Introduction

The aim of the work presented here was to provide insight into geomechanical and corresponding mineralogical alterations to the MX-80 bentonite under variable THC exposure scenarios that are relevant to the canister/barrier interface within a deep geological disposal facility for nuclear waste.

Correlation of the mineralogical alterations with changes in the measured engineering parameters has seldom been conducted with previous research focusing specifically on one of these aspects; more usually the mineralogical alterations. This work attempts to bring both aspects into consideration on a consistent data set with the goal of determining the impact upon the barrier system. The engineered barrier system (EBS) is a multi-barrier passive system that is widely considered for most national geological disposal concepts [1–7]. The EBS for the UK's current concept for disposal of intermediate (ILW) and high level wastes (HLW) is comprised of the waste matrix (vitrified, processed nuclear waste), the waste container (presently considered to be S275 carbon steel), the intermediate compact clay barrier (MX-80, Na-bentonite) and the outer host rock. The purpose of the engineered barrier is to isolate the radioactive waste, prevent canister displacement or breach due to externally imposed stresses and retard long-life radionuclide transport in the long-term. These functions are achieved by ensuring a low permeability, ductile and self-healing environment, provided by the high swelling and unique physicochemical nature of the MX-80.

Low permeability can be achieved through high compaction of the bentonite resulting in very slow ground water movement, and ensuring diffusion controlled flow regime, the rate of which is found to be an important aspect of the overall integrity of the containment system [4,5].

The physicochemical properties of the bentonite include a large double diffuse layer (DDL), large negative layer charge and gelling properties that further play a part in maintaining a low permeability. Furthermore, the bentonite can retain radionuclides by physicochemical absorption on the edge and basal planes of the clay platelets [3,8–10].

It is also well established that bentonite displays a high swelling characteristic that is a function of the aforesaid physicochemical properties related to the montmorillonite mineral [3,11–14]. The high swelling capacity provides an effective mechanism for the barrier to retard and adsorb radionuclides as well as the ability to self-heal to ensure fissure closure.

Therefore, the optimum density during compaction needs to be fully achieved to enhance the EBS effectiveness, as the dry density is a function of the material's swelling pressure/volumetric capacity upon hydration. Density loss of the clay barrier over the life-span of the system must be kept to a minimum to uphold its design function. It is considered that near-field variables such as corrosion, accessory mineral dissolution and re-precipitation, high saline groundwater and heat caused by the fission products may negatively impact the favourable properties. During storage, temperatures after emplacement are likely to reach 100 °C at the canister/bentonite interface, although peak canister array temperatures are dependent on the design of each national concept [2,10,15,16]. It is anticipated that the heat will initially drive-off ground water at elevated temperatures causing drying and redistribution of salts within the barrier away from the interface [5]. The inferred near-field transitional phases were expressed within the NAGRA reports (NARGRA is the Swiss Technical centre for the national GDF concept) [2,15] and these key stages in the physicochemical evolution of the interface were simplified here for the purpose of understanding the system. The following stages were used to aid in the identification of the condition of the sample when subject to specific environmental conditions as well as to determine the thermal and chemical boundaries: (1) Aerobic—highest thermal conditions resulting in an initial dry phase with dry oxidation of the steel occurring; (2) Aerobic—resaturating conditions with temperatures dropping allowing gradual ingress of groundwater along with hydroxide development of the steel canister; (3) Anerobic—saturated conditions with mid to low temperatures in the long-term with reduction of hydroxides along with hydrogen production. The experiments investigated environmental factors such as salinity, temperature and corrosion that were derived from the inferred environmental conditions in order to assess the impact of these on the intrinsic geomechanical and physicochemical characteristics of the bentonite. Samples were allowed to naturally evolve within a sealed environment with oxic conditions initially being present (similar to conditions following barrier placement). While it was difficult to quantitatively control redox conditions the sample was kept in an isolated environment with exposure to steel, saline concentration/composition and thermal

loading/duration varied. Thus, as will be the case for a barrier, any oxidation which did occur, consumed the limited oxygen available within the isolated system.

2. Experimental Method

Several batch tests have been conducted over a comprehensive temperature range, between 20–300 °C. The initial temperatures were chosen for initial characterisation purposes as the upper limit of 100 °C has been selected for the current UK disposal concept. The thermal upper-limit has been also expressed in many technical and safety case reports [7,17–19]. Higher temperature testing was implemented as a comparative study to see if any significant alterations started to occur once beyond the 100 °C boundary under the time scales imposed by the experimental study. These higher thermal loading scenarios along with the use of more complex electrolytic solutions were considered necessary for experimental exploration. It is widely thought that higher temperatures may succeed in yielding potential alterations that would naturally occur over geological time-scales at lower temperatures due to the activation energies involved. The alterations were measured with respect to the geomechanical and physicochemical properties and compared to the "unaltered" material properties. Most of the batch tests were run within pyrex glass beakers that were sealed, firstly to prevent excess moisture evaporation for the duration of the THC exposure (Figure 1) and secondly, to limit access of oxygen into the system, thereby promoting the consumption of available oxygen and, depending on the thermodynamic constrains, inducing reducing conditions. Heated consignments involving steel and/or saline solutions were conducted on a hot plate and powder tests, or constant volume tests, investigating corrosion exposure, thermal exposure and duration were conducted within a thermostatic oven. These were either allowed to dry over time or sealed within a constant volume cell (Figure 2).

Figure 1. Heated thermo-saline-corrosion exposure samples.

The experimental conditions were varied to gain a broad spectrum of situational circumstances. All pilot batch samples, expect for batch #3, could free swell upon hydration with no volumetric constraint imposed. Generally, most pilot batch tests were only exposed to the experimental variables for a duration of 1-month, however batch tests 5–8 were run for 4, 12 and 24 months respectively. This was to gain a profile of the effects of thermo-chemical exposure and duration. Ultimately, the primary experimental variables in the batch tests were electrolytic concentration and composition, compaction state, the presence of Fe(0) in the form of a carbon steel coupon (80 mm diameter) and thermal loading and duration.

Figure 2. From Batch test #4 (For 1 month duration, sample containing Steel/Mx-80 & distilled water), compacted and heated to 100 °C within a sealed constant volume cell (Ø: 50 mm, h: 20 mm).

The principle saline solution consisted of NaCl with a UK specific concept reference concentration of 0.45 M (0.45 M NaCl SAFE barrier reference concentration (~×1 sea water)) implemented for most tests. To consider the impact of other salts in a mixed groundwater, additional experiments were conducted with a more complex saline solution, including Na^+, K^+ and Ca^{2+} with concentrations taken from groundwater data obtained from the Eastgate borehole and representative of a crystalline host rock [20] (Table 1). A ratio of experimental solution to clay mass of 10 was implemented, based on previous studies by Guillaume et al. [21], as a suitable systematic concentration ratio replicating the interface environment. The experimental regime is outlined in Table 2.

Table 1. Calculated salt concentrations for a crystalline rock mass at 995 m BGL [20].

Salt	Concentration (Molar)
NaCl	0.34
KCl	0.135
$CaCl_2$	0.017

Upon completion of the THC exposure, the samples were processed and prepared for the allocated post testing protocol of geomechanical and physicochemical testing (Table 2). Samples that contained carbon steel were dissected and separated at the zone of visible corrosion integration with the respective portions of the sample tested in order to understand the geomechanical and geochemical evolution over the sample profile. NaCl concentrations for the first two batch tests were increased in increments of 0.225 M. The concentrations used were 0.225 M, 0.45 M, 0.675 M and 0.9 M in order to achieve a spread of results over a large range of salinities.

3. Post Exposure Testing

Geotechnical measurements consisted of Atterberg limits conducted in accordance with BS1377-2:1990 and swell index measurements in accordance with ASTM D5890 standards. Addtionally, Cation Exchange Capacity (CEC) and X-ray Diffraction (XRD) analyses were conducted to suppliment the geotechnical measurements.

Table 2. Experimental Regime (PI: Plasticity index, SI: Swell index, CEC: Cation exchange capacity, XRD: X-ray diffraction).

Batch Code	Batch Test Consignment	Description	No. of Samples	Duration (Days)	Temp (°C)	Post Analysis
1	Saline profiling	• Increasing Saline Concentration Solutions (DI Water (×3) for and ×3 per NaCl, KCl and CaCl Respectively) • Mass Ratio: 10	12	30	20	SI, PI
2	Steel-Clay-Saline	• Increasing NaCl Concentration With MX-80 and Steel Coupon (×3 DI Water Plus ×3 for NaCl at 0.225 M, 0.45 M, 0.675 M and 0.9 M) • Mass Ratio: 10	15	30	20	SI, PI
3	High Temperature Steel-Clay-De-Ionised (DI) water	• MX-80, S275 Steel Coupon with DI Water Only at 27% (%wt) • Sealed Batch Cells • Mass Ratio: 10	3	30	105	SI, PI
4	Thermal Loading and Duration Tests (No Steel, No Salt)	• Thermal Loading Tests Over 24 h • Thermal Duration Tests at 105 °C • ×3 per Duration and Thermal Load	39	1, 4, 7, 14, 30, 56, 84	20, 50, 70, 90, 110, 150	SI, PI, CEC
5	Thermal Loading and Duration with High Saline Solution (No Steel)	• Powder Samples Each with NaCl, KCl, CaCl and a Synthetic Groundwater Solution Mix 27% (%wt) • Investigating Thermal Load and Duration with Salt	15	56, 84	20, 100, 150	SI, PI, CEC
6	Steel-Clay-Saline Under Very High Thermal Loading and Prolonged Duration	• Varied Boundary Conditions i.e., Steel/Clay with DI Water, Steel/clay with Synthetic Groundwater, Clay with Synthetic Groundwater and Clay with DI Water	24	120	20, 150	SI, PI, XRD
7	1-Year Steel/Clay Interaction Tests	• MX-80, S275 Steel with DI Water	3	365	20	SI, PI
8	2-Year Steel/Clay Interaction Tests (No Saline Solution)	• MX-80, S275 Steel with DI Water	3	730	20	SI, PI

3.1. Atterberg Limits

Atterberg limits were measured in compliance with BS1377 Pt: (2) and were conducted on samples post THC exposure at room temperature. Samples were dried, hand ground, passed through a 425 μm sieve and re-mixed with deionised water to consistencies that meet the plastic limit and liquid limit sample requirements. The liquid limit measurements used approximately 300–400 g of bulk material. A cone penetrometer apparatus was used to measure four penetration points over an increasing moisture range. Subsequently the line of best fit plotted through the points gave the liquid limit corresponding to 20 mm of cone penetration. The plastic limit sample used approximately 10–20 g of dry material. The sample was rolled into a 3 mm thread until cracking occurred transversely and longitudinally, at which point the moisture content was determined, corresponding to the plastic limit. The difference between the two values gives the plasticity index which is a measure of the range of moisture content that a soil can take and still exhibit shear resistance as well as volumetric change; the higher the PI the more expandable the clay.

3.2. Swell Index

Swell index measurements conformed to the American standards D5890-11 for free swell volume measurements of compacted clay liners used in landfill applications. The sample was dried in a thermostatically controlled oven at 105 °C ± 5 °C, hand ground in an agate mortar and then a dry mass of 2 g, passing a 150 μm sieve, was taken. To conduct the test a 100 mL graduated cylinder-class A, with 1 mL subdivisions, was filled with either deionised water or NaCl solution (depending on the test, relating to the sample's experimental history) to the 90 mL mark. Subsequently the 2 g mass was added in increments of 0.1 g over 10 min intervals, allowing each mass increment to saturate and deposit to the bottom. Once all of the mass was added the remaining 10 mL of liquid was added, thus washing in any particles on the glass into the solution. The sample was allowed to free swell/saturate over a 16–24 h period, upon which the volume of the clay was measured in mL. The overall free swell index measurement is expressed as mL/2 g $\equiv$ Cm^3/2 g of dry material.

3.3. CEC

The Cation Exchange Capacity (CEC) is a method widely used in soil analysis to measure the material's ability to retain positively charged ions e.g., Mg^{2+}, Ca^{2+}, K^{+}, Na^{+} etc. In the case of the engineered barrier around the HLW/SF canister this determines the potential to retain/sorb radionuclides from potential leachate. Cations are electrostatically held within the interlayer of the clay platelets and are exchanged by replacing power of the lyotropic series. The method used in this study was the barium chloride method to ISO 11260—standardised in 1994.

3.4. XRD

XRD analysis was conducted on a PANalytical X'Pert Pro Multi-Purpose Diffractometer fitted with an ultra-fast X'Celerator detector and using a Cu anode (operated at 40 kV and 40 mA) to generate Cu-Kα radiation (0.15418 nm). A step size of 0.167° was used with a (nominal) counting time per step of 250 s over a scan range of 2–30° 2q. The ICDD PDF-4 Minerals 2015 Database was used to identify crystalline phases in bulk samples. The samples, after hand grinding, were put into clay/deionised water suspension with a concentration between 57–60 mg/mL to ensure that they were smooth and thick enough to allow mineralogical homogeneity [22].

In order to fully differentiate the minerals present (given that many minerals share similar d-spacings) several types of XRD analyses were conducted i.e., bulk, oriented air dried, oriented glycolated and oriented heat treated at 440 °C and 550 °C respectively, with a scan range between 2–30 (2θ). For oriented sample analysis, the clay slurries were mounted on glass slides.

Firstly, the bulk analysis enabled the determination of non-clay constituents such as iron-rich minerals, Fe oxide-hydroxides, quartz, feldspars etc. Subsequent orientation of the specimens allowed

analysis of the clay component with air dried samples being used as the reference. Glycolation of the samples at 40 °C was used to differentiate expandable phyllosilicates from Mg-bearing minerals (i.e., vermiculites) that tend to show similar d-spacings (in the region of 14 Å). Solvation causes an expansion of the interlayers in smectitious materials and an increase in the d-spacing to approximately 18 Å that is not seen in vermiculites [22]. This procedure can therefore enable insight into the bentonite's ability to swell under the effects of THC exposure. Finally, the heat treatment of the material to induce a collapsed state due to thermal dehydration/decomposition also helps to differentiate particular minerals both via the d-spacing and as an indicator for the determination of precursor minerals due to the development of pseudomorphs.

4. The Material Description

MX-80 bentonite used within this study was in powdered form, commercially known as Bentonex WB, a Wyoming Na-bentonite supplied by RS minerals® (RS minerals® is a UK based limited company which specialises in supplying a large range of clay minerals and salts for agricultural and industrial use). It is a homoionic smectite, the general composition of which is presented in Table 3.

Table 3. Bulk composition of MX-80 [23].

Mineral Type	% Wt.
Montmorillonite	94
Gypsum	≤1
Feldspars	≤4
Quartz	≤2

The composition of the bentonite clearly displays a high proportion of montmorillonite with some micro aggregates. This is expected for a naturally occurring material. The unit cell formula for the MX-80 given by [5] (Equation (1)), also displays the relative proportions of Fe^{3+} and Fe^{2+} bound within the octahedral layer.

$$(Na_{0.3})(Al_{1.55}Mg_{0.24}{Fe^{3+}}_{0.20}{Fe^{2+}}_{0.01})(Si_{3.96}Al_{0.04}) \quad (1)$$

4.1. Geotechnical Classification

Standard geotechnical tests (liquid limit, plastic limit, particle size distribution, swell index) were conducted to characterise the unaltered MX-80 as described in Section 3 above. The results presented here (Table 4) were used as control parameters to be compared to the THC affected samples. Given the relatively high values, the material is a high swelling and highly active material. The high plasticity index, a function of the liquid limit and plastic limit, indicates that the material is prone to large volume changes while maintaining shear strength when undergoing saturation. The ability for the material to remain sufficiently stiff (i.e., to limit canister displacement) as well as its ability to swell (i.e., self-healing of fissures) is satisfied by this bentonite due to its highly active characteristics. MX-80 is a clay that displays thixotropic and highly swelling characteristics over a very large range of moisture content. This gives the material the unique ability to seal up any potential flow pathways and remain sufficiently ductile to enable stress redistribution that may develop during the working life of the barrier. These geomechanical properties, when coupled with the physicochemical characteristics i.e., a large CEC, indicates that bentonite is a suitable candidate material that will retard and slow groundwater movement and radionuclide migration. Additionally, the compact bentonite can demonstrate favourable rheological characteristics thus acting as a stress buffer for any large scale displacements of the host rock or canister.

Table 4. Geotechnical measurements for unaltered MX-80.

Material	LL (%)	PL (%)	PI (%)	% CLAY (≤2 μm)	Activity	SI (Cm^3/2 g)
RS® MX80	397	32	365	89.41	4.08	28

The swell index tests were implemented to quantify the volumetric free swelling capacity upon hydration, expressed as mL/2 g (≡ cm^3/2 g). Through examination of Figure 3, the MX-80 is highly expansive particularly when compared to Ca-homoionic bentonite, which has also been considered for use within barrier systems [12,24].

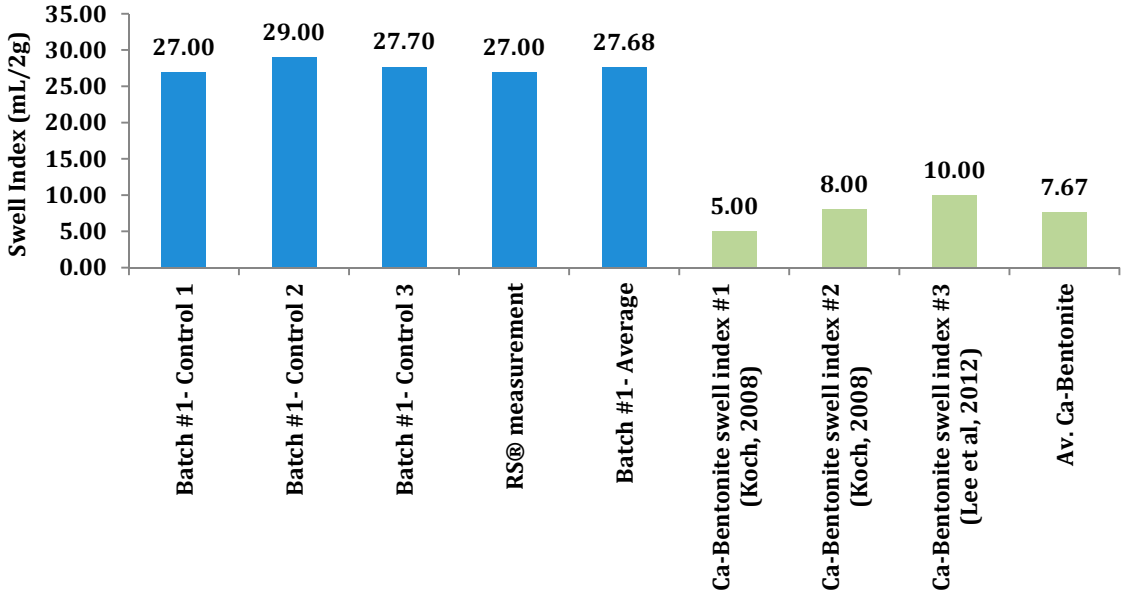

Figure 3. Control swell index results, along with a comparison to a Ca-type bentonite.

4.2. Physicochemical Classification

Figure 4 presents the bulk XRD analysis of the RS® MX-80. The smectite component displays a d-spacing of approximately 10 Å, indicating that the material was in a state of zero hydration. Quartz and cristobalite appear to be abundant (≈3.34 Å, 4.04 Å respectively). Zeolite is also thought to be present, generally due to the sharp peaks and specifically due to the peak at 4.47 Å (Moore and Reynolds, 1997). The peak at 3.18 Å indicates the presence of a plagioclase feldspar along with calcite at ≈2.55 Å. The shoulder towards the right of the calcite peak may indicate a Lo-crystobalite or pyrite peak overlap (≈2.45 Å). There is also a broad peak around ≈4.7 Å, which may indicate the presence of feldspar or chlorite.

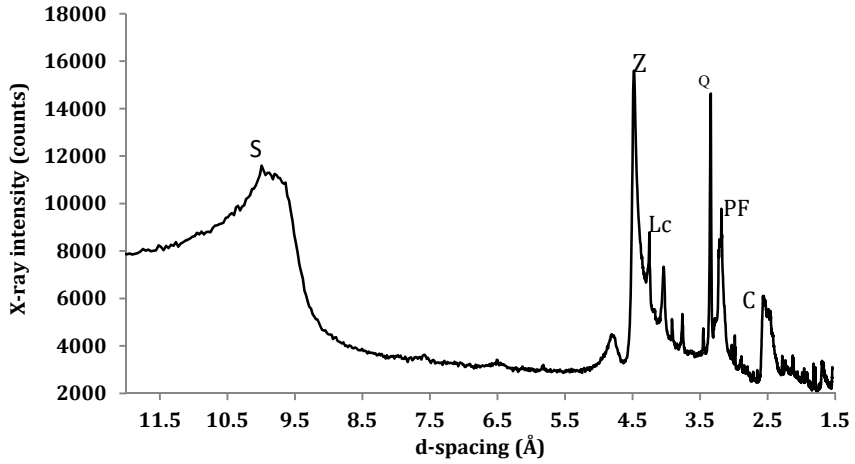

Figure 4. Bulk XRD run on the RS® MX80 (S: Smectite, Lc: Lo-cristobalite, Z: Zeolite, Q: Quartz, PF: Plagioclase feldspar, C: Calcite).

Figure 5 displays the oriented XRD profiles. It is observed that there is a prominent peak at 12.5 Å, for the air-dried sample, with a subsequent jump to 17 Å upon glycolation. This confirms the presence of the high-charge smectite [22].

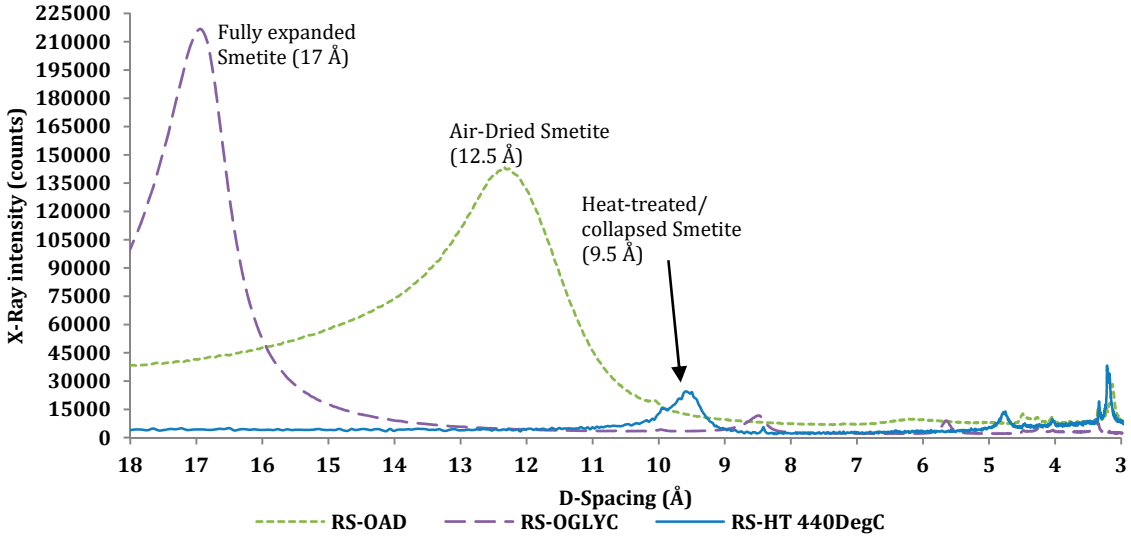

Figure 5. Oriented air-dried, glycolated heat-treated XRD on the MX80.

Examination of the 002/003 intensity ratio can also be used to infer the abundance of Fe within the octahedral sheet [22]. The 002/003 intensity ratio indicates the magnitude of back-scattering from the incident X-rays i.e., higher intensity ratios indicate higher amounts of Fe present. From Figure 6, the intensity ratio is 1.3. Comparing this with data from Moore and Reynolds (1997) (Table 5) indicates that there is a small amount of Fe present and confirms the content profile given by Wilson et al. (2010) (Equation (1)).

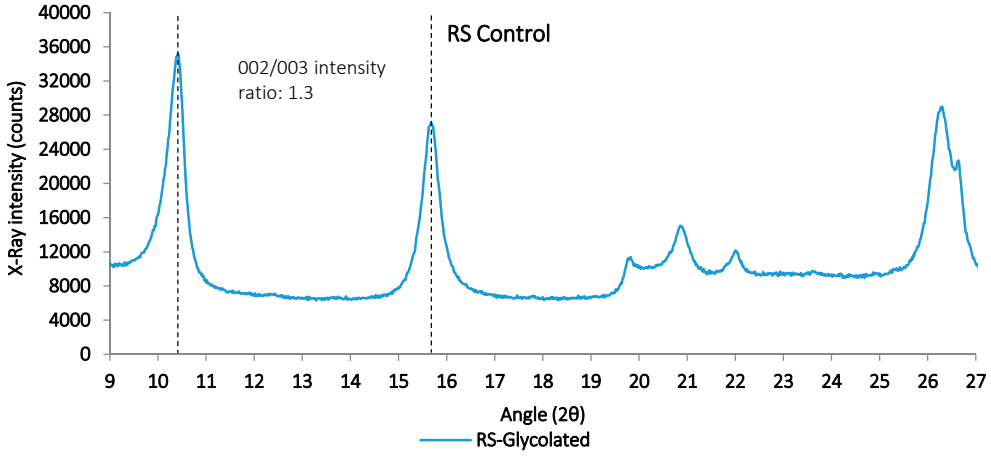

Figure 6. 002/003 intensity ratios for the RS® control.

Table 5. Fe content and intensity ratios for MX-80 with comparison of common smectite minerals [22].

Mineral Type	Fe Content per Two Octahedral Sites	Intensity Ratio
MX-80 used in study	0–0.5	1.3
Nontronite	1.7	9.5
Saponite	0–0.5	1.5
Pure Montmorillonite	0.1	0.7

CEC measurements of the unaltered MX-80 resulted in an average CEC of 70 ± 10 (mEq/100 g). This indicates that the material displays a favourable property of retardation and sorption of mobile radionuclides in comparison to other clays, due to large negative layer charge [10,25–30].

5. Results and Discussion

5.1. Batch 1—Saline Interaction/Profiling Tests

The MX-80 was subjected to saline solutions for approximately one month under ambient conditions (20 °C). The purpose was to isolate and investigate the impact of low to high saline concentrations of NaCl, KCl and CaCl solutions on the engineering function of the MX-80. These salts were chosen due to their prevalence in deep groundwater [20] and furthermore because it is thought that illitisation due to K fixation is one potential alteration pathway [31]. The measured free swell index is plotted along with the results from [12] for comparison to Ca-bentonite, the second most considered bentonite (Figure 7).

Lee et al. [12] state that the slight increase observed for Ca-bentonite between 0.05 and 0.1 M NaCl is due to the exchange of Ca^{2+} ions with Na^{+} ions increasing the diffuse double layer in the interlayer. The intra-aggregate pore-water is driven into the inter-lamella spacing under an osmotic gradient in dilute NaCl solutions. However, higher electrolyte concentrations reduce the osmotic pressure causing the collapse of interlayers, this corresponds to a reduction in the DDL. Consequently, this diminishes the material's ability to swell on a macro level. The MX-80 still intrinsically exhibits a higher swelling capacity over the entire saline range for NaCl and KCl solutions, even at the reference concentration (0.45M). However, using a higher valence cation as the dominant electrolyte i.e., CaCl, large reductions in the DDL and bulk swelling capacity are observed. Overall, there was a drop in swell index of 52%, 49% and 81% for NaCl, KCl and CaCl respectively at the concept reference concentration. A similar pattern was seen for the plasticity index (Figure 8).

The overall characteristic bulk volumetric capacity of the clay as well as its plastic behaviour has been impeded with increasing salt concentration, with the clay becoming progressively more inert. Concentrations between zero and 0.45 M seem have the highest impact on the plasticity and swelling

capacity for all electrolyte solutions. Further increase in saline concentration continues to reduce these properties, but to a lesser extent.

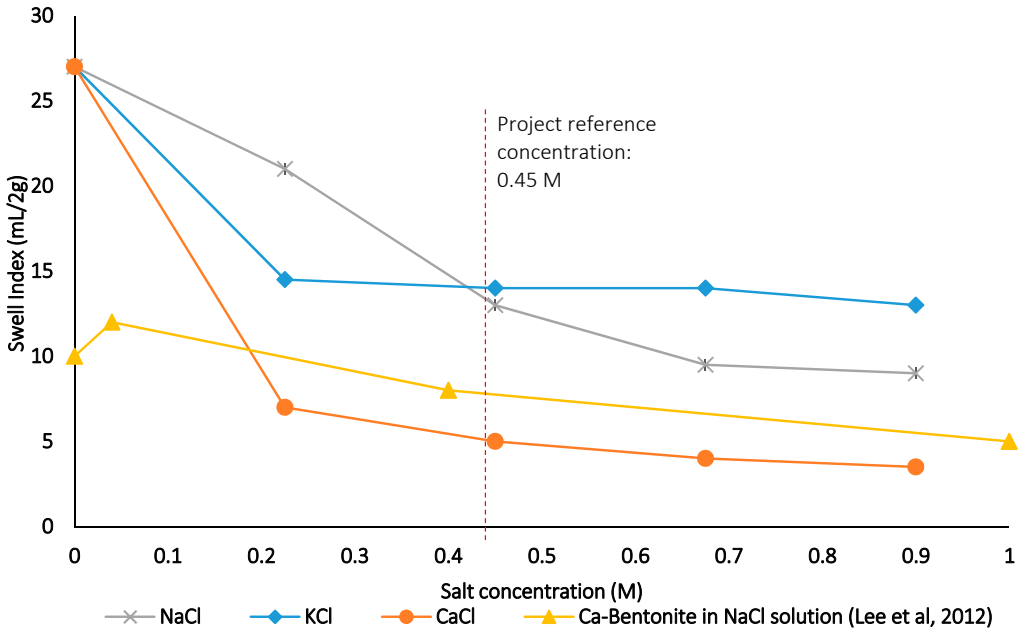

Figure 7. Swell index results for batch 1 tests (Ca-bentonite results after 19), dotted line highlighting the reference salinity concentration.

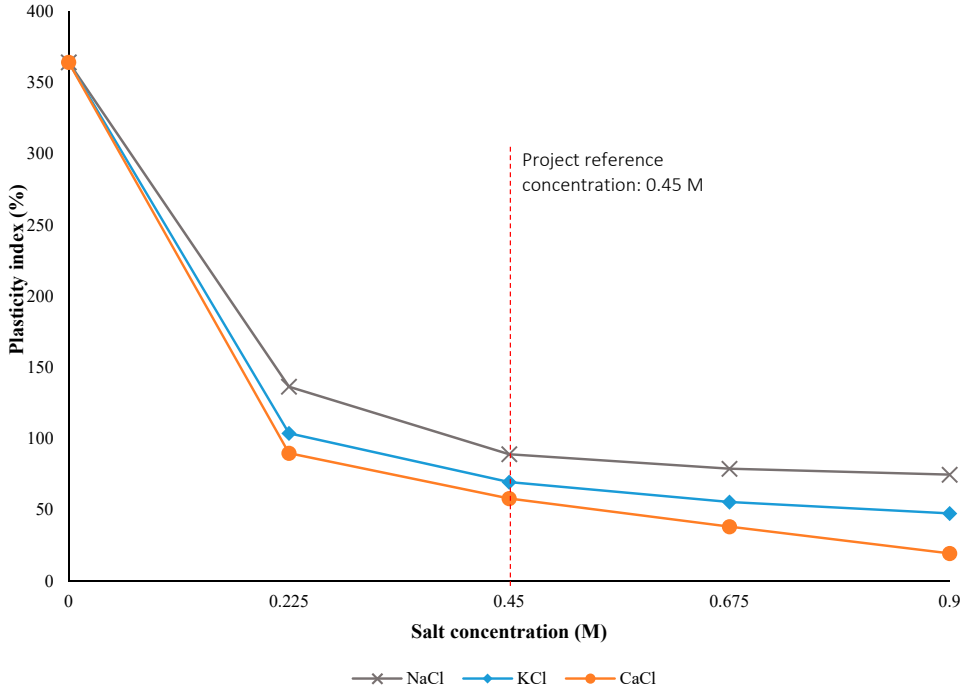

Figure 8. PI vs. Saline solution concentration batch 1 tests (Dotted line indicates reference salinity).

Nonetheless, the activity of the clay (swell index) remains at 1 or above, which is considered in soil mechanics as an "active clay" [32].

Figures 7 and 8 illustrate the preferential exchange of cations within the interlayer based on the lyotropic series i.e., the CaCl induces the most significant impact on the DDL. Increasing the

concentration of the salt within solution causes a lower osmotic pressure, thereby inducing collapse between platelets. This also indicates that the probability of K fixation is increased for Na-bentonite in K-rich systems.

5.2. Batch 2—Steel-Clay-Saline Interaction under Ambient Thermal Conditions

This batch test introduced the carbon steel, type S275 (in the form of a 2 cm × 2 cm coupon inserted into the beaker), into the MX-80 and investigated the interaction of corrosion, distilled water and low to high saline solutions (NaCl) with MX-80 at 20 °C for a duration of 1 month. Redox conditions were not controlled during THC exposure and post-mortem sampling was separated by the zone of visible corrosion precipitation to allow an alteration profile to be formed. Figure 9, displays the free swell index for this batch series. Two measurements were taken from the sub-sampled zones at less than 3 mm and greater than 3 mm from the steel interface.

It appears that the outermost section of the sample (>3 mm) is affected by the saline solution displaying the characteristic reduction with increasing saline concentration seen in Batch #1 (20% reduction at the reference concentration). However, the sub-sampled zone closed to the steel has an increased SI in the mid saline range (+17%). Fe-corrosion products are known to have a higher volume compared to when they are in a zero-valent state [33] and the increased SI is likely attributable to this.

Corrosion was seen to have migrated more into the bentonite in the mid-salinity concentration range as compared to 0.0 M and 0.9 M concentrations (Figure 10). At low to mid concentrations (0.225 and 0.45 M) the loss in thixotropic characteristics and an increase in ion mobility is likely, allowing more free movement/diffusion of corrosion products throughout the intra-lamellae pores. Whereas at high saline concentrations (0.675 and 0.9 M) the particles flocculate and densify the bulk material, thereby reducing the diffusion rate.

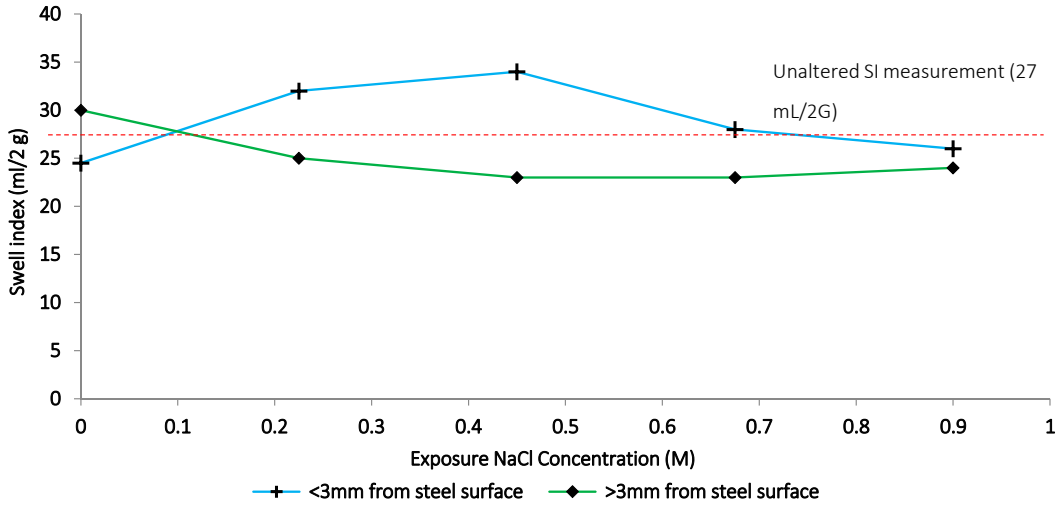

Figure 9. Swell index results for batch #2 (dotted line indicates the control free swell value).

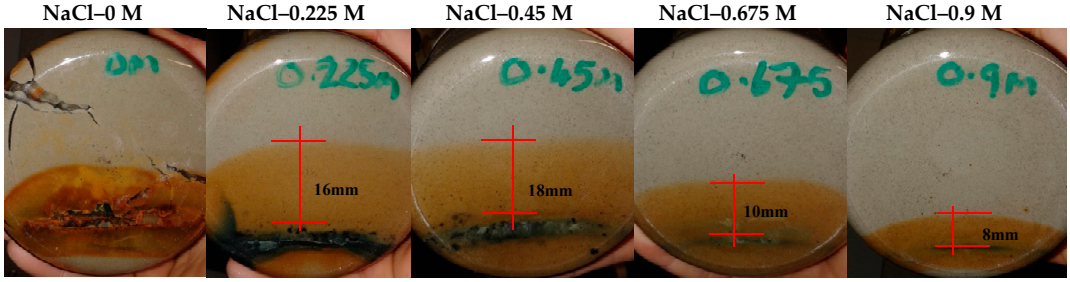

Figure 10. Extent of corrosion integration under ambient conditions after 1-month exposure.

5.3. Batch 3—High Temperature Steel-Clay-De-Ionised (DI) Water

This batch test further investigated the interaction between corrosion products and the MX-80 under elevated thermal exposure without the presence of saline pore-water. Tests were conducted for 1 month with DI water to observe the impact of corrosion products. A comparison can be made between the 0.0 M sample under ambient conditions and the results for this batch to assess the influence of corrosion and temperature (Figure 11).

Interestingly, samples that contained no saline pore-water did not exhibit the increase in volumetric capacity at the interface and the associated reduction in the outer zone as seen in Batch #2 for mid saline concentrations (Figure 9). Instead, it appears that the corrosion products at the interface inhibit the swell index with a slight increase in the outer zones that is accentuated by exposure to higher temperatures. These observations correlate to the findings of [34–36] and the alterations are likely due to the impact of temperature on the DLL and dielectric constant.

Furthermore, corrosion products within the bentonite in the non-saline environment result in low diffusion away from the interface with high concentration of hydroxides that may cause cementation and potential substitution of Fe [37]. This is due to the impact of the salt solution on the gelling and thixotropic consistency of the MX-80 forming a barrier against the diffusion of Fe ions.

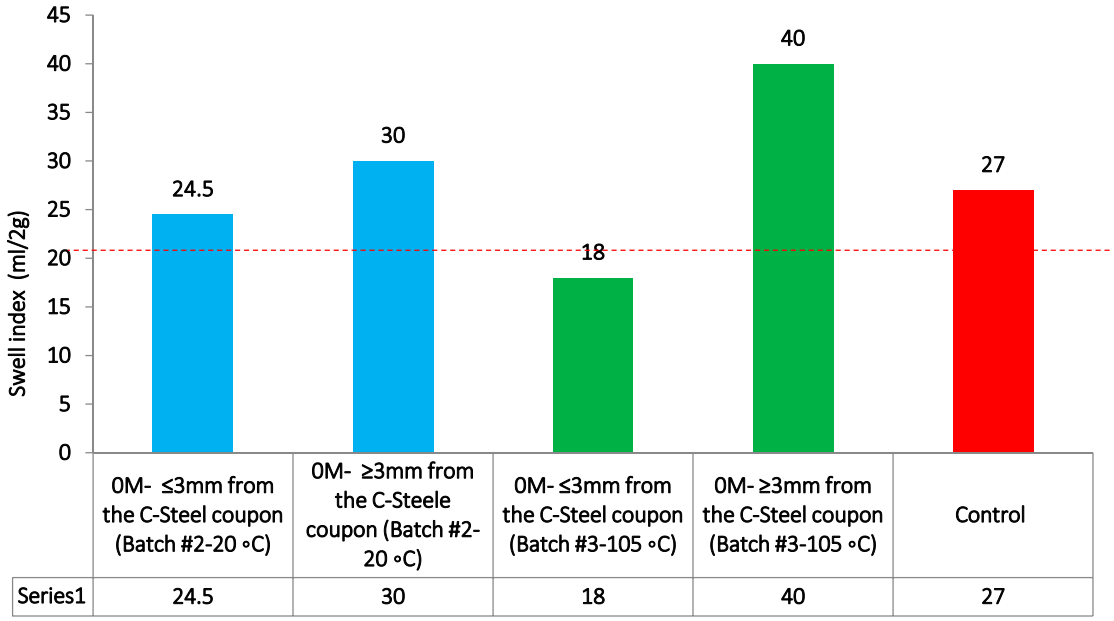

Figure 11. Swell index results for batch #3 with a comparison to batch #2 0 M measurements at 20 °C.

5.4. Batch 4 & 5—Impact of Thermal Loading and Duration

Two types of tests were conducted to observe the influence of temperature on the physical characteristics of the MX-80. The first type (thermal loading) subjected the MX-80 to fixed temperatures for a 24 h period. Six temperatures between 50 °C and 150 °C were tested (at 20 °C increments) with a further three temperatures tested up to 300 °C. The second type (thermal duration) investigated the impact of length of exposure to high thermal loading with the MX-80 subjected to 105 °C for seven different durations between 1 day and 12 weeks.

The free swell index results for the thermal loading tests are presented in Figure 12. Interestingly, the free swell of the MX-80 remains relatively unaltered up to a temperature of 90 °C (Point a, Figure 12) after which it increases in the temperature range up to 150 °C (Point b, Figure 12), reaching a maximum increase of 27%. This increase is likely attributable to the increased DDL due to a thermally reduced surface potential charge [34–36] and it may be noted that the results correlate well with the swelling index results in batch 3 (Figure 10).

In the temperature range above 150 °C the free swell capacity of the MX-80 declines with increasing temperature, reaching a maximum decrease of 22% at a temperature of 300 °C (the highest temperature tested). This drop is likely a result of the elevated temperatures inducing fusing of platelets due to the precipitation of siliceous minerals and the development of disordered amorphous crystallites [37].

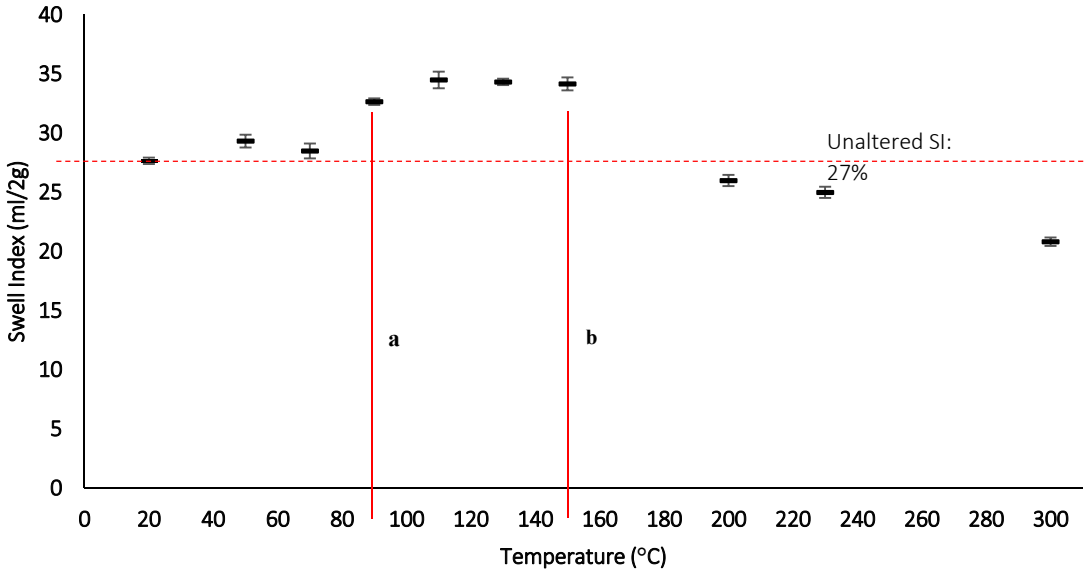

Figure 12. Swell index measurements with increasing thermal exposure after 24 h, a: lower temperature point where SI increases, b: upper temperature point where after which the SI reduces.

In contrast, the plasticity index measurements, which might be expected to show similar results to swell index, showed very little variation (Figure 13), although the trend may be interpreted to be consistent with swell index (showing a very slight increase in the range 90 °C–150 °C) followed by a decrease to 300 °C). Thus, despite significant changes in swelling behaviour the material retains its ability to resist shear during uptake of water.

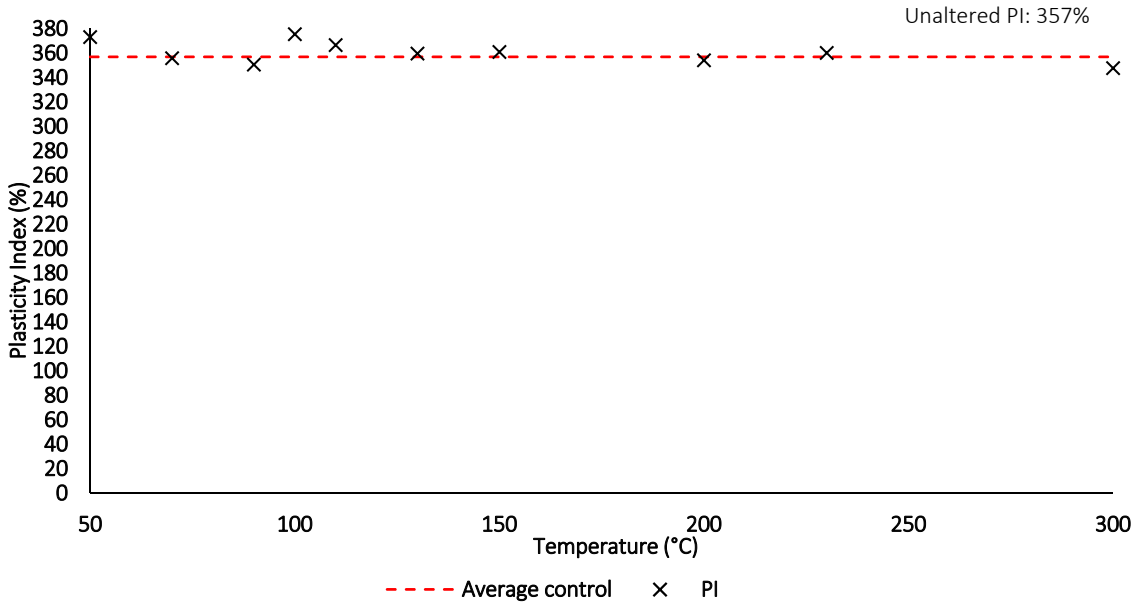

Figure 13. Plasticity index with increasing thermal exposure for 24 h.

The thermal duration test results (at 105 °C) are presented in Figures 13 and 14. The observed increase in the swell index for shorter duration exposures (Figure 14) correlates with the measurements in Figures 10 and 11 under the same temperature load. However, this increase is short-lived and longer durations within this thermal range begin to reduce the swelling capacity.

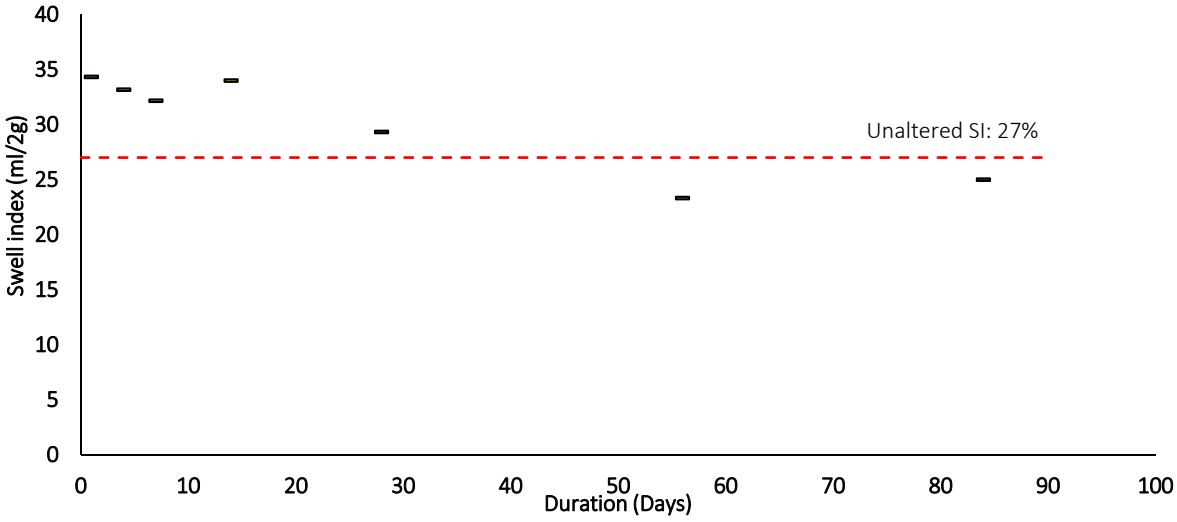

Figure 14. Swell index after Thermal loading (105 °C) and duration.

The plasticity index displays a similar trend (Figure 15) although it begins to drop earlier on than the swell index and continues to drop up to the longest duration tested at 84 days, with a measured reduction of 32%.

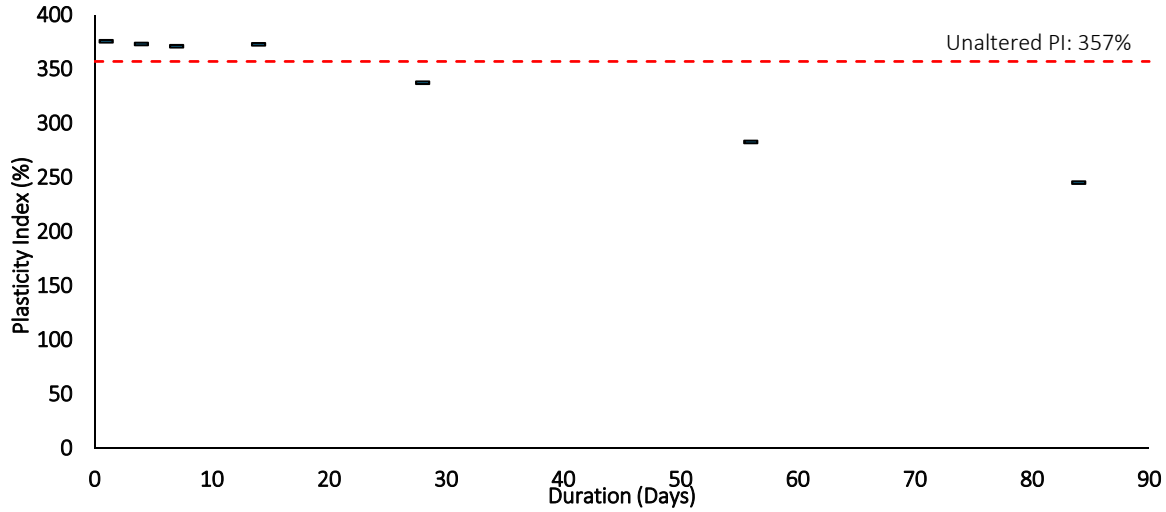

Figure 15. Plasticity index after Thermal loading (105 °C) and duration.

Overall the thermal exposure initially increases the DDL and layer charge, however longer durations appear to induce alteration and have a greater influence on the consistency of the bentonite than high thermal loading over very short time-scales. With respect to the functionality of the barrier, any loss in swelling capacity or PI indicates a reduction in the materials ability to "self-heal" or maintain sufficient plastic characteristic with respect to canister positioning and rheology. However, the time-scales considered here were relatively short in the context of a geological disposal facility

(GDF) and a loss of 32% in PI after 86 days does not infer that the parameter will continue to linearly decay. This process will be further limited by the temporal decay of interface temperatures.

CEC measurements were also conducted after loading and duration testing (Figures 16 and 17). Short-term thermal loading (Figure 16) displays negligible change to the layer charge characteristics of the MX-80, even at temperatures of 300 °C, confirming the conclusions above. However, for the duration measurements (Figure 17) the CEC profile follows those of the SI and PI measurements (Figures 14 and 15), supporting the premise that there is some alteration to the layer charge with increasing thermal duration. The influence will again be limited by the thermal decay of the interface over time.

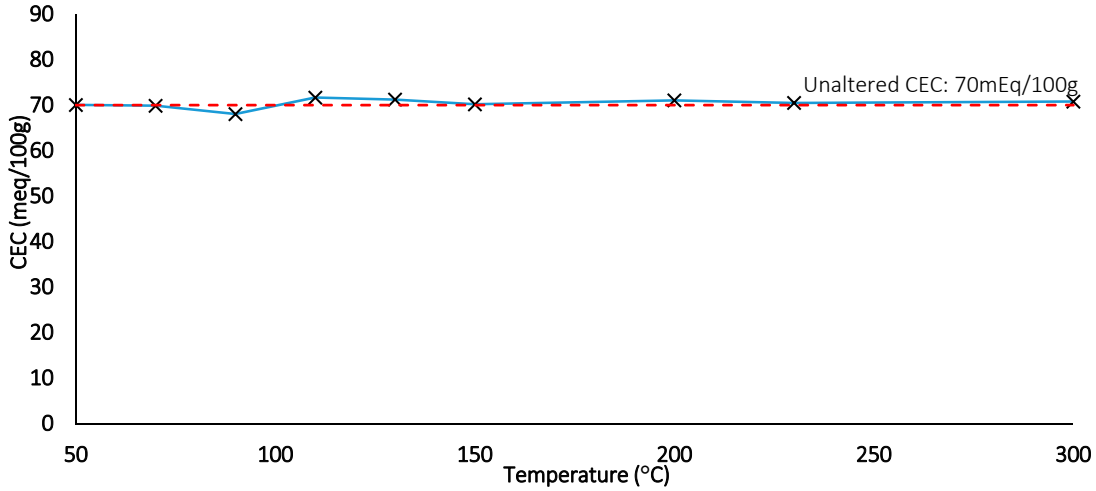

Figure 16. CEC measurements for thermal loading tests (Dotted line: control).

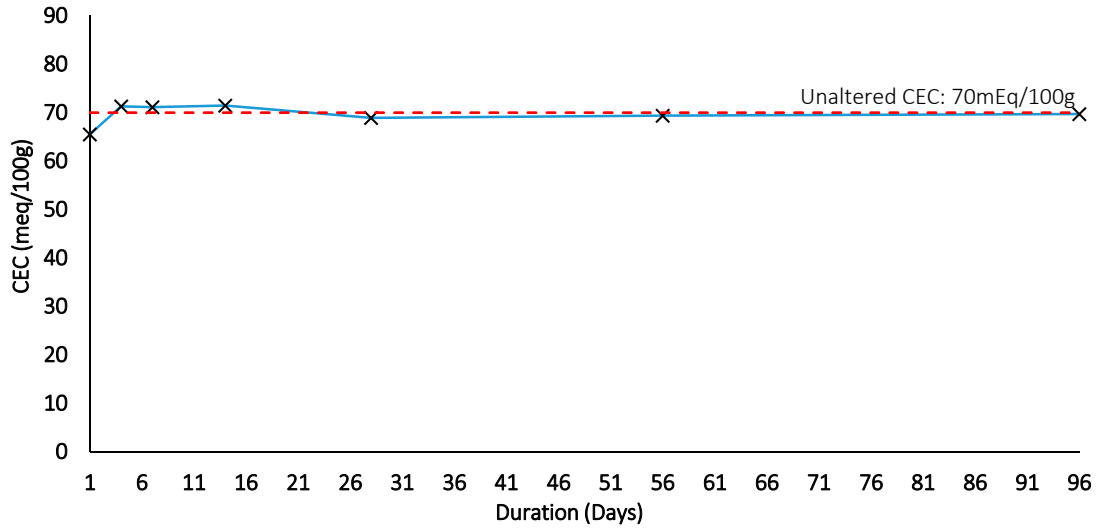

Figure 17. CEC measurement for thermal duration tests (Dotted line: control).

5.5. Batch 6—Steel-Clay-Saline Exposure under Elevated Temperatures and Prolonged Duration

The interaction between bentonite and carbon-steel, with and without synthetic groundwater, under ambient and elevated temperatures (20 °C and 150 °C), over a prolonged period (4 months) was investigated. The post exposure swell indices for the various scenarios are displayed in Figure 18.

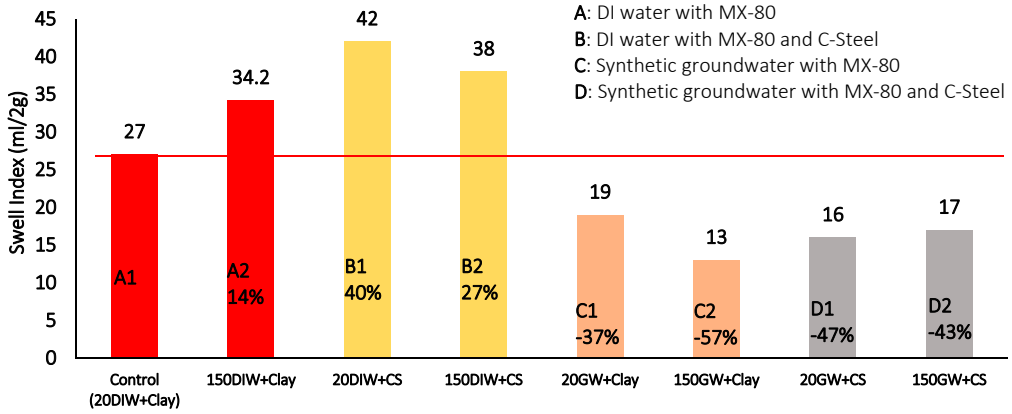

Figure 18. Swell index measurements at 20 °C and 150 °C for combinations of MX-80, De-Ionised water or synthetic groundwater and carbon steel (The number before the batch code represents the maximum thermal exposure temperature, the lettering system refers to the key, above, for a description of each batch configuration).

The swell index is seen to increase in the presence of temperature alone (A2) where four months of high thermal exposure resulted in an increase in swell index of 27% over that of the control. It is also seen to increase more (~50%) in the presence of carbon steel plus DI water with or without temperature (B1 & B2). This observation is consistent with the results of batches 2, 3, 4 and 5, and is thought to be due to the combination of the thermal effects on the layer charge and DDL thickness as well as the integration of high volume (iron) hydroxides (steel corrosion products). The high salinity experiments (C & D) clearly indicate the impact of the synthetic groundwater in reducing the swell index, and it may be additionally noted that only a minor difference was observed between corrosion and no-corrosion samples. The effect of elevated temperature in conjunction with high salinity groundwater increases the reduction in free swell from −30% (C1) to −52% (C2).

The impact of high salinity and temperature compared to the lesser influence of corrosion products is further demonstrated in Figure 18 for plasticity index where the effects are like those noted for swell index. However, it may also be seen that the presence of corrosion products does not increase plasticity in the way it did for swell index (B1 and B2).

A technical report for SKB ([38] Document reference: TR-10-15, 2010) states that the plasticity index must not drop below 283% for the Swedish disposal concept. Evidently the presence of temperature and saline solutions with or without steel lowers the PI considerably below this limiting value, and, in this context, it may be concluded that even short-term thermo-saline exposure may be significant.

In addition to the swell index and plasticity tests above, XRD analysis was conducted on the interface (<3 mm from the steel) and outer zones (>3 mm from the steel) of the batch samples to determine if there was significant mineralogical and accessory mineral alteration. The three stages of XRD analysis were conducted; air-dried, glycolated and heat treated. The d-spacing of the glycolated mineral components are given below (Table 6).

Table 6. d-Spacing of the glycolated clay components.

Batch #	d-Spacing (Å)
Control	**17**
20DIW+CS	16.9
150DIW+CS	16.8
20GW+Clay	16.9
150GW+Clay	16.7
20GW+CS	16.9
150GW+CS	16.9

The smectite component, and its ability to retain radionuclides, is not compromised under the explored conditions as the measured d-spacings for each exposure test are comparable to that of the unaltered MX-80.

However, under air-dried conditions, the synthetic groundwater batch that included clay and no corrosion products (D1 and D2) displayed a peak shift from 12 Å to ~15 Å (Figure 19), with an increased effect in the higher temperature sample. This is characteristic of divalent interlayer cation exchange [21,22]. The exchange rate is clearly increased by the thermal loading, due to increased kinetics from thermal expansion of the interlayer, kinematic viscosity of the solution as well as the increased activation energy of the system. It is clear from this peak shift (Figure 20) and the geomechanical results from batch 1 that divalent cation exchange significantly inhibits the swelling and plasticity of the MX-80. Calcium in solution is preferentially exchanged and this exchange is accelerated under higher temperatures. This is evident by the macro swell index and plasticity measurements. However, the intrinsic layer charge is not altered as demonstrated by the glycolated d-spacing.

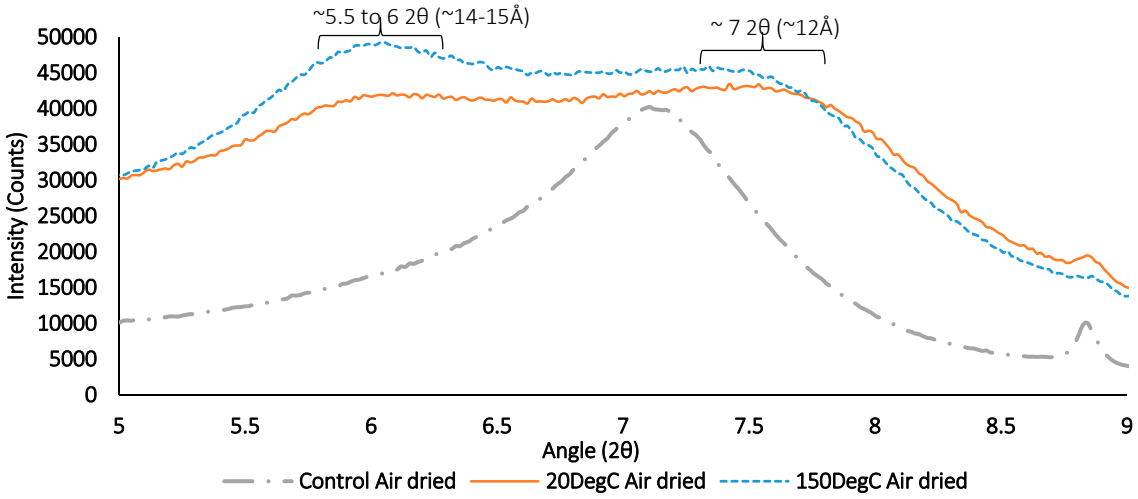

Figure 19. XRD results for air-dried sample containing synthetic groundwater and clay only with no corrosion products. Exposed to ambient temperature (20 °C) and elevated temperature (150 °C) respectively.

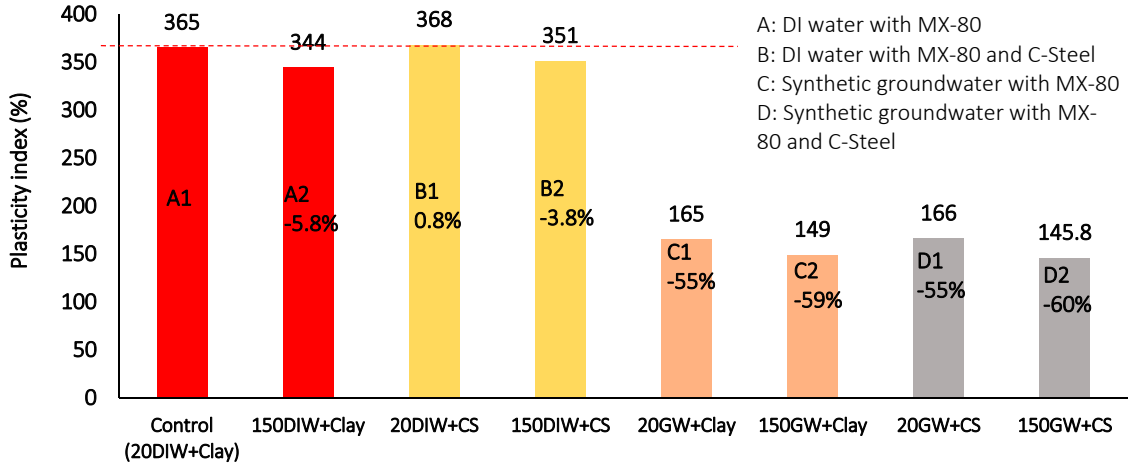

Figure 20. Plasticity index results at 20 °C and 150 °C for combinations of MX-80, De-Ionised water or synthetic groundwater and carbon steel. (The number before the batch code represents the maximum thermal exposure temperature, the lettering system refers to the key, above, for a description of each batch configuration).

The 002/003 peak intensity ratios were also compiled from the XRD results to determine changes in iron content (Table 7). The results indicate that there is no increase in exchange of Fe^{3+} in the octahedral layer, particularly for the samples containing the steel coupons. This indicates that under the explored conditions and time constraints, no Fe integrated into the octahedral sheet. This is supported by the unaltered layer charge exemplified by the glycolated d-spacings.

Table 7. Compiled 002/003 peak intensity ratios for each batch consignment.

Batch	002/003 Intensity Ratio
Control	1.3
20 °C, DI Water, MX80 and c-steel	1.1
150 °C, DI Water, MX80 and c-steel	1.4
20 °C, Groundwater and MX80 only	1.1
150 °C, Groundwater and MX80 only	1.1
20 °C, Groundwater, MX80 and c-steel	1.1
150 °C, Groundwater, MX80 and c-steel	1.1

5.6. Batch 7 and 8—Corrosion/MX-80 Interaction over Long-Term Durations

These tests investigated the long-term interaction between carbon steel and MX-80. The thermal exposure was kept low (20 °C) and DI water was used to observe the integration of the corrosion products into the bentonite matrix. The consignments were run for a duration of 1 and 2 years respectively.

Figure 21, displays a comparison between the two batch consignments. This demonstrates that the corrosion products integrated into the bentonite had only minor impact on the free swell capacity of the MX-80. However, the observed increase for the 1-year batch sample is most likely due to the presence of (iron) hydroxides, similar to what was seen in the duration tests (batches 4 and 5) although the effect has manifested for longer here due to the presence of corrosion products (as in batch test 6) and the lower temperatures.

The slight reduction after 2-years is also similar to what was seen in the duration tests although here the swelling effect of hydroxides may have been counteracted in time as the samples appeared to develop anaerobic corrosion cells where the hydrated bentonite formed a seal, allowing only oxygen within the immediate zone of the steel to be consumed.

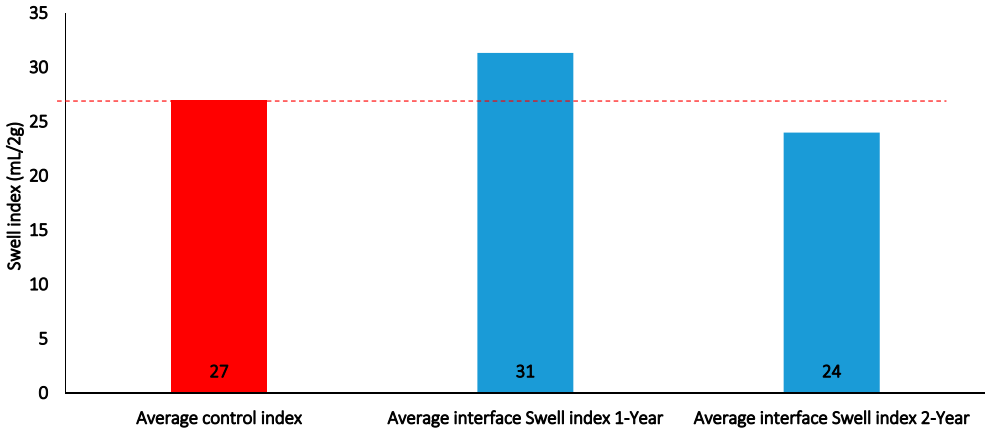

Figure 21. Interface swell index for 1 and 2-year batch tests.

This was characterised by a variation in the colour of the diffused corrosion front through the bentonite, ranging from blueish/green, suggestive of a reducing/anoxic, Fe^{2+}-rich environment penetrating the bentonite by approximately 20 mm from the interface, to orange in the outer regions, suggestive of an Fe^{3+}-rich front (Figure 22).

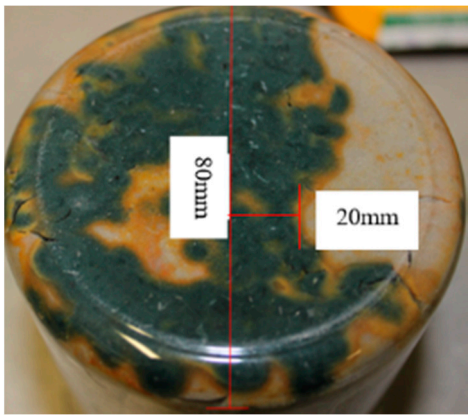

Figure 22. Development of Greenish-blue corrosion with an Orange corrosion front after 2 year.

The mobility and integration of Fe^{2+} ions into the smectite structure in the anaerobic environment near the interface could cause an alteration of the layer charge and an increase in lattice stress [4,39,40] thereby inhibiting the swelling capacity of the MX-80.

Figure 23 displays the plasticity index for both consignments. Again, a trend corresponding to previous batch test results is observed. After 2-years the reduction of the Plasticity Index by 22% indicates that the temporal dimension is an important factor in the interaction between the corrosion products and the bentonite as well as possible integration of Fe into the bentonite structure under reduced conditions. Since the plasticity index is a function of the bulk and dry masses of the clay, the more corrosion products contained within the bentonite then the greater the effect on the results. This is evident in the gradual reduction in the PI in time, which affects the material's ability to resist shear, and most importantly it may be seen to be approaching the minimum value set for the SKB concept ([38] Document reference: TR-10-15, 2010).

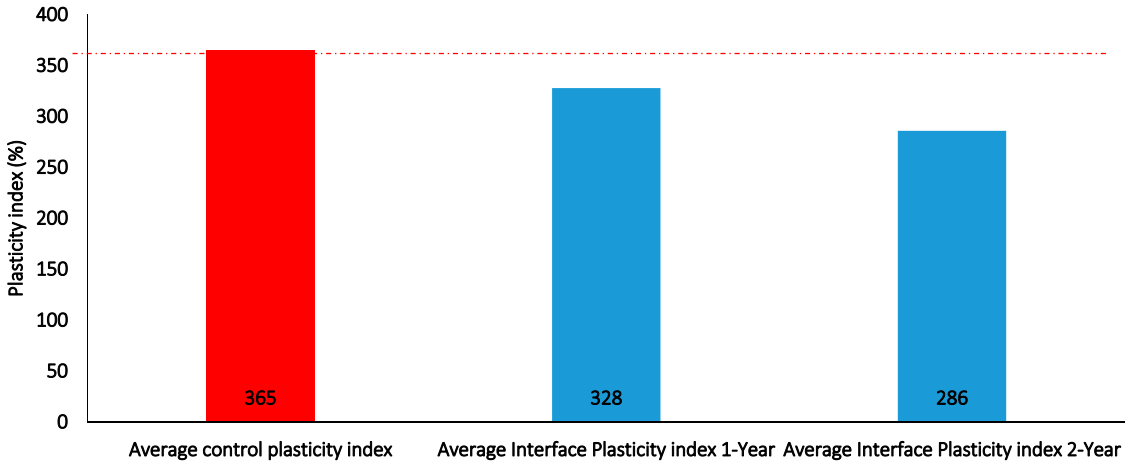

Figure 23. Interface plasticity index for 1 and 2-year batch tests containing DI water only.

It is clear that temperature aids the rate of kinetics, but the most significant results are displayed when comparing the longer duration tests to the 4-month exposure test (Figure 24). Table 8 displays the corresponding depth of corrosion integration vs. exposure time. It must be noted that the bentonite was in an uncompact/non-volume constrained system and therefore it was not necessarily representative of the EBS barrier conditions. Maintaining the bentonite in a relatively confined system will yield different spatial diffusion magnitudes due to the lower porosity when in a compact/confined state.

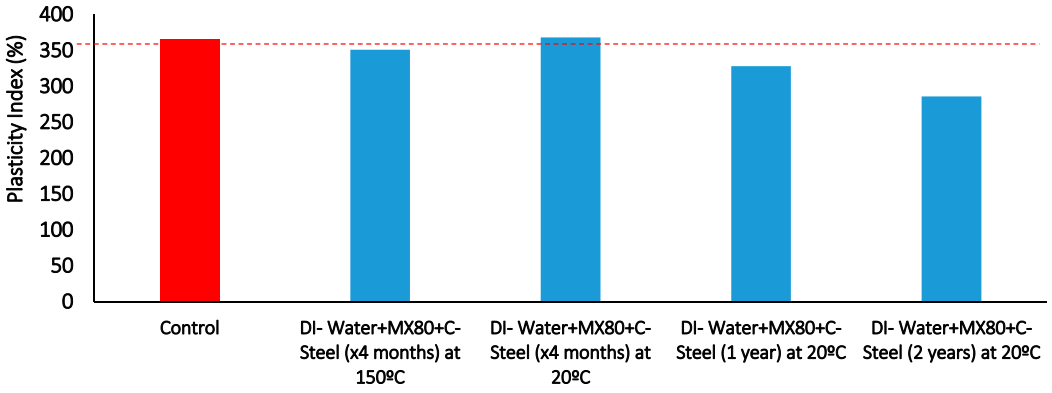

Figure 24. Plasticity index results comparison of duration vs. Carbon-steel/bentonite interface exposure at 20 °C, also includes one 150 °C result for comparison.

Table 8. Plasticity index results comparison of duration vs. Carbon-steel/bentonite interface exposure at 20 °C with Deionised water.

Batch (DI Water + MX-80 + Carbon-Steel)	Extent of Visible Corrosion Integration (mm)
Control	0
4 months at 20 °C	15
1 year at 20 °C	20
2 years at 20 °C	35

6. Conclusions

This study has allowed insight into the combined and time-dependant nature of temperature, corrosion and salinity on the engineering function of the engineered barrier with consideration to a UK specific disposal concept.

Specifically, this work examined the influence of salinity, temperature loading and duration and corrosion on the intrinsic geomechanical and geochemical properties of the MX-80 bentonite considered for use within the EBS. Experimental conditions were varied with respect to near-field conditions that are predicted to be present during the working life of the EBS. A series of batch tests were conducted with post-test geomechanical measurements looking at plasticity and swellability. XRD and CEC analyses was also conducted to explore the intrinsic physicochemical alterations and enable correlation with the bulk geomechanical measurements. Unlike most previous works that concentrated on one of these aspects, through a consistent set of geomechanical and geochemical examinations it was possible to determine the direct cause of deviation from the intended engineering function of the barrier with respect to the physicochemical evolution.

The data presented indicate that salinity alone has an instantaneous negative impact on the MX-80's ability to free swell and maintain its plasticity, thereby reducing its capacity to self-heal. Short-term exposure to saline concentration at the reference salinity (0.45 M-NaCl) reduces the swelling ability by approximately 50%. However, the impact of higher valence cations, such as calcium can reduce the material's swell index by 82% at a concentration of 0.45 M. Thus, it may be concluded that the specific hydro-chemical environment of a GDF site may be critical in controlling the geomechancial performance of the bentonite barrier.

It was also found that both peak temperature and duration of thermal exposure affect the geomechanical behaviour of the bentonite. Thermal loading at the concept reference peak temperature (105 °C) was shown to reduce the swell index and plasticity index of the bentonite as the duration of exposure increases although short-term thermal loading initially causes an increase in swelling capacity due to the increased dilation coefficient and changes to the dielectric constant for highly saturated bentonite [34,41]. A measured drop in swelling capacity at higher temperatures (≥150 °C)

as well as over longer durations ($\geq$ 1 month) is thought to be due to the combined effect of particle fusing, by dissolution and re-precipitation of siliceous minerals, and reduction of the layer dielectric constant [27,34,37].

Tests conducted on multiple variations of saline solutions under varied temperatures and durations in the presence of carbon steel, indicate that high salinity groundwater influences the barrier much more than corrosion products or temperature alone. Geochemical analyses showed that the presence of corrosion products (iron oxy-hydroxides) did not result in iron exchange in the octahedral layer of the clay but rather indicate the formation of poorly crystalline corrosion products within the clay matrix. In the short-term, these had a positive effect, increasing swelling capacity, but in the longer-term (1 and 2 years) a negative impact on the swelling capacity was seen, likely due to alteration of the layer charge and an increase in lattice stress [4,39].

Further geochemical analysis demonstrated that higher temperatures resulted in higher disordering of the smectite and secondary mineral composition. However, the swelling component remained largely equivalent to and characteristic of high-charge smectite, meaning that the material's ability to adsorb radionuclides as well as the barriers ability to "self-heal" would not be significantly affected. Samples containing the synthetic groundwater solution showed a predominant interlayer exchange of Ca and divalent interlayer occupation was observed. However, no alteration to the layer charge was detected, indicating that no structural alteration had occurred within the clay. Therefore, the observed geomechanical alterations were caused by interlayer cation occupation, the results clearly demonstrated that bulk geomechanical behaviour was dominated by alterations to the interlayer occupancy than alteration to the clay itself. It appears that longer THC exposure plays a significant role in the corrosion interaction with the bentonite. Whereas, short-term alterations are more related to the presence of high saline solutions as well as thermal loading/exposure impacting the interlayer charge, which reduced the materials consistency and swelling capacity with increasing concentration and thermal exposure.

Acknowledgments: The authors would like to express appreciation to Stuart Patterson and Fred Beadle for their technical support during experimental work. The authors recognise the funding received from the EPSRC (SAFE Barriers—EP/I036427/1) as well as patronage from Radioactive Waste Management Limited (RWM) (http://www.nda.gov.uk/rwm), a wholly-owned subsidiary of the Nuclear Decommissioning Authority. RWM is committed to the open publication of such work in peer reviewed literature, and welcomes e-feedback to rwmdfeedback@nda.gov.uk.

Author Contributions: Christopher Davies conducted the main experimental analysis as well as compiled and composed the main text and data. Colin Davie was project PI and proof-read, edited and provided technical support on the geotechnical aspects. Both Maggie White and Alasdair Charles contributed to the corrosion/clay mineral identification and analysis aspects of the paper.

Conflicts of Interest: The authors declare no conflicts of interest.

References

1. Hella, P.; Pitkänen, P.; Löfman, J.; Partamies, S.; Vuorinen, U.; Wersin, P. *Safety Case for the Disposal of Spent Fuel at Olkiluoto—Definition of Reference and Bounding Groundwaters, Buffer and Backfill Porewaters*; Posiva Report 2014-04; Posiva: Eurajoki, Finland, 2014.
2. Leupin, O.X. *Montmorillonite Stability under Near-Field Conditions*; NAGRA Technical Report 14-12; NAGRA: Wettingen, Switzerland, 2014.
3. Galamboš, M.; Rosskopfová, O.; Kufčáková, J.; Rajec, P. Utilization of Slovak bentonites in deposition of high-level radioactive waste and spent nuclear fuel. *J. Radioanal. Nucl. Chem.* **2011**, *288*, 765–777. [CrossRef]
4. Kumpulainen, S.; Kiviranta, L.; Carlsson, T.; Muurinen, A.; Svensson, D.; Sasamoto, H.; Yui, M.; Wersin, P.; Rosch, D. *Long-Term Alteration of Bentonite in the Presence of Metallic Iron*; SKB Technical Report TR-10-527; SKB: Solna, Sweden, 2010.
5. Wilson, J.C.; Savage, D.; Bond, A.; Watson, S.; Pusch, R.; Bennett, D. *Bentonite—A Review of Key Properties, Processes and Issues for Consideration in the UK Context*; NDA-RWMD Report QRS-13788ZG-1; Quintessa Limited: Oxford, UK, 2010.

6. Watson, S.; Metcalfe, R.; McEwen, T.; Paulley, A. *International Precedents for HLW/SF Iron Canister Concepts*; Quintessa Report QRS-1376A-1; Quintessa: Oxfordshire, UK, 2007.
7. Wersin, P.; Johnson, L.H.; McKinley, I.G. Performance of the bentonite barrier at temperatures beyond 100 °C: A critical review. *Phys. Chem. Earth* **2007**, *32*, 780–788. [CrossRef]
8. Galamboš, M.; Krajňák, A.; Rosskopfová, O.; Viglašová, E.; Adamcová, R.; Rajec, P. Adsorption equilibrium and kinetic studies of strontium on Mg-bentonite, Fe-bentonite and illite/smectite. *J. Radioanal. Nucl. Chem.* **2013**, *298*, 1031–1040. [CrossRef]
9. Galamboš, M.; Suchánek, P.; Rosskopfová, O. Sorption of anthropogenic radionuclides on natural and synthetic inorganic sorbents. *J. Radioanal. Nucl. Chem.* **2012**, *293*, 613–633. [CrossRef]
10. Delage, P.; Cui, Y.-J.; Tang, A.M. Clays in radioactive waste disposal. *J. Rock Mech. Geotech. Eng.* **2010**, *2*, 111–123. [CrossRef]
11. Saba, S.; Barnichon, J.D.; Cui, Y.J.; Tang, A.M.; Delage, P. Microstructure and anisotropic swelling behaviour of compacted bentonite/sand mixture. *J. Rock Mech. Geotech. Eng.* **2014**, *6*, 126–132. [CrossRef]
12. Lee, J.O.; Lim, J.G.; Kang, I.M.; Kwon, S. Swelling pressure of compacted Ca-bentonite. *Eng. Geol.* **2012**, *129–130*, 20–26.
13. Herbert, H.; Kasbohm, J.; Sprenger, H.; Fernández, A.M.; Reichelt, C. Swelling pressures of MX-80 bentonite in solutions of different ionic strength. *Phys. Chem. Earth* **2008**, *33*, 327–342. [CrossRef]
14. Karnland, O.; Olsson, S.; Nilsson, U.; Sellin, P. Experimentally dermined swelling pressures and geochemical interactions of compacted Wyoming bentonite with highly compacted Wyoming bentonite with highly alkaline solutions. *Phys. Chem. Earth* **2007**, *32*, 275–286. [CrossRef]
15. Landolt, D.; Davenport, A.; Payer, J.; Shoesmith, D. *A Review of Materials and Corrosion Issues Regarding Canisters for Disposal of Spent and High-Level Waste in Opalinus Clay*; NAGRA Technical Report 09-02; NAGRA: Wettingen, Switzerland, 2009.
16. Madsen, F.T. Clay mineralogical investigations related to nuclear waste disposal. *Clay Miner.* **1998**, *33*, 109–129. [CrossRef]
17. Holton, D.; Dickinson, M.; Hoch, A.; Cowper, M.; Thetford, R.; Allinson, H.; Johnson, M. Project Ankhiale: Disposability and full life cycle implications of high-heat generating UK wastes. In *NDA/Amec report*; Report no: RP51; AMEC: Cheshire, UK, 2012.
18. Karnland, O. *Long Term Test of Buffer Material at the ASPO HRL, LOT Project*; Technical Report- TR-09-31; SKB: Stockholm, Sweden, February 2011.
19. King, F.; Watson, S. *Review of the Corrosion Performance of Selected Metals as Canister Materials for UK Spent Fuel and/or HLW*; Report no: QRS-1384J-1; Quintessa Limited, Henley-on-Thames: Oxfordshire, UK, July 2010.
20. Manning, D.A.C.; Younger, P.L.; Smith, F.W.; Jones, J.M.; Dufton, D.J.; Diskin, S. A deep geothermal exploration well at Eastgate, Weardale, UK: A novel exploration concept for low-enthalpy resources. *J. Geol. Soc.* **2007**, *164*, 371–382. [CrossRef]
21. Guillaume, D.; Neaman, A.; Cathelineau, M.; Mosser-Ruck, R.; Peiffert, C.; Abdelmoula, M.; Dubessy, J.; Villieras, F.; Baronnet, A.; Michau, N. Experimental synthesis of chlorite from smectite at 300 °C in the presence of metallic Fe. *Clay Miner.* **2003**, *38*, 281–302. [CrossRef]
22. Moore, D.M.; Reynolds, R.C., Jr. *X-ray Identification of Clay Minerals*; Oxford University Press: New York, NY, USA, 1997.
23. RS®Minerals. MX-80 Delivery Specification Sheet. Available online: http://www.rsminerals.co.uk/bentonite (accessed on 10 August 2017).
24. Koch, D. European bentonite as alternatives to MX-80. *Sci. Technol. Ser.* **2008**, *334*, 23–30.
25. Roxburgh, I.S. *Geology of High-Level Nuclear Waste Disposal—An Introduction*; Chapman and Hall: New York, NY, USA, 1987.
26. Bergaya, F.; Lagaly, G. (Eds.) *Handbook of Clay Science*; Elsevier: Oxford, UK, 2006.
27. Gomez-Espina, R.; Villar, M.V. Geochemical and mineralogical changes in compacted MX80 bentonite submitted to heat and water gradients. *Appl. Clay Sci.* **2010**, *47*, 400–408. [CrossRef]
28. Idiart, A.; Maia, F.; Arcos, D. *Geochemical Evaluation of the Near-Field for Future HLW Repository at Olkiluoto*; Posiva Report 2013-05; Posiva: Eurajoki, Finland, 2013.
29. Bradbury, M.H.; Berner, U.; Curti, E.; Hummel, W.; Kosakowski, G.; Thoenen, T. *The Long Term Geochemical Evolution of the Near-Field of the HLW Repository*; NAGRA Technical Report 12-01; NAGRA: Wettingen, Switzerland, 2014.

30. Wilson, J.C.; Benbow, S.; Sasamoto, H.; Savage, D.; Watson, C. Thermodynamic and fully-coupled reactive transport models of a steel-bentonite interface. *Appl. Geochem.* **2015**, *61*, 10–28. [CrossRef]
31. Wersin, P.; Birgersson, M.; Olsson, S.; Karnland, O.; Snellman, M. *Impact of Corrosion-Derived Iron on the Bentonite Buffer within the KBS-3H Disposal Concept*; SKB Technical Report. Report No: TR-08-34; Svensk Kärnbränslehantering AB: Stockholm, Sweden, 2008.
32. Craig, R. *Craigs Soil Mechanics*, 7th ed.; CRC Press: London, UK, 2004.
33. Scully, J.C. *The Fundamentals of Corrosion*, 3rd ed.; Pergamon Press: Oxford, UK, 1990.
34. Mitchell, J.K.; Soga, K. *Fundamentals of Soil Behavior*, 2nd ed.; John Wiley & Sons Inc.: Hoboken, NJ, USA, 2005; 577p.
35. Adamcova, J.; Kolaoikova, I. *Alteration Processes in Bentonites: Mineralogical and Structural Changes during Long-Term and Short-Term Experiments*; Mineralogy and Mineral Resources—Faculty of Science and the Czech Geological Survey: Prague, Czech Republic, 2006.
36. Arasan, S.; Yetimoglu, T. Effect of inorganic salt solutions on the consistency limits of two clays. *Eng. Environ. Sci.* **2008**, *32*, 107–115.
37. Liu, X.; Prikryl, R.; Pusch, R. THMC—Testing of three expandable clays of potential use in HLW repositories. *Appl. Clay Sci.* **2011**, *52*, 419–427.
38. Svensk Karnbranslehantering AB (SKB). *Design and Initial State of the Buffer*; Technical Report: TR-10-15; SKB: Stockholm, Sweden, 2010.
39. Wersin, P.; Birgersson, M.; Olsson, S.; Karnland, O.; Snellman, M. *Impact of Corrosion-Derived Iron on the Bentonite Buffer within the KBS-3H Disposal Concept—The Olkiluto Site as a Case Study*; NAGRA Technical Report 2007-11; NAGRA: Wettingen, Switzerland, 2007.
40. Stucki, J.W.; Golden, D.C.; Charles, B.R. Effects of oxidation state of octahedral iron on clay swelling. *Clays Clay Miner.* **1984**, *32*, 357–362. [CrossRef]
41. Tang, A.-M.; Cui, Y.J.; Barnel, N. Thermo-mechanical behaviour of a compacted swelling clay. *Geotechnique* **2008**, *58*, 45–54. [CrossRef]